

Integration of Smartphones Into Small Unmanned Aircraft Systems to Sense Water in Soil by Using Reflected GPS Signals

Mehmet Kurum¹, Senior Member, IEEE, Md. Mehedi Farhad, and Ali Cafer Gurbuz², Senior Member, IEEE

Abstract—We investigate the feasibility of using built-in GNSS sensors within ubiquitous smartphone devices from a small UAS for the purpose of land remote sensing. We summarize the experimental findings and challenges that need to be resolved in order to perform the GNSS reflectometry (GNSS-R) technique via smartphones. In late 2018, a series of experiments were conducted and designed by integrating two smartphones into a multicopter UAS by attaching them to ground plates to isolate and record both direct and reflected GNSS carrier-to-noise density ratio (C/N_0) separately. It was demonstrated that, first, fluctuations of moving GNSS specular reflections are correlated with spatial ground features with appreciable dynamic range and second, radiation pattern of the smartphone's inbuilt antenna has a significant effect on the received signal strength. In 2020, more experiments were conducted to examine the quality of in-built chip and antenna of a smartphone with regard to the GNSS-R approach as well as the consistency of measurements. These follow-up experiments involved, first, placement of the smartphone on a pan-tilt mechanism on a tripod, second, formation flights with smartphone on a gimbal and a high-quality custom-built dual-channel GNSS-R receiver, and, third, flying the UAS at different times of the day on two consecutive days. It was demonstrated that, first, the radiation pattern of the smartphone's GNSS antenna are observed to be highly irregular, but time-invariant, and, second, internal GNSS chip produces observables of sufficient quality, and, third, the fluctuations of the reflected signal are repeatable under the same configuration at different times.

Index Terms—Android, GNSS raw data, GNSS reflectometry (GNSS-R), signals of opportunity, smartphones.

I. INTRODUCTION

GNSS Reflectometry (GNSS-R) is an innovative technique that exploits reflected GNSS signals (multipath) for remote sensing of the environment [1], [2]. In this scheme, the GNSS transmitters which provide free illumination, and the receiver that captures the reflected signals can be considered as a multistatic radar system. This technique has been gaining attention in the remote sensing community since it only requires the development of small size weight and power—cost passive

receivers, an analysis algorithm, and no on-board transmitter [3]. Over the past two decades, various methods have been developed to estimate the geophysical parameters such as ocean surface winds [4], snowpack, and sea ice [5], soil moisture [6]–[10], vegetation [11]–[13] as well as wetland and flooding monitoring [14]–[16]. In particular, application and validation of the GNSS-R technique over land surfaces have been accelerated as a potential microwave remote sensing alternative with the launch of new spaceborne missions [17]–[19] in recent years. A number of studies have used geodetic or specially designed GNSS receivers from airborne [6], [8], [10], [13]–[16] and tower-based platforms [7], [9], [11]. They have experimentally demonstrated that reflected GNSS signals from land are highly sensitive to water content in the soil and vegetation type and amount over ground. The experimental findings have also been supported by modeling studies [20]–[23].

The potentiality of the GNSS-R studies has mostly been investigated through custom-built, expensive systems or network of geodetic receivers that are mostly fundable through space agencies, universities, research institutes, or large corporations. There have been a small number of studies that use low-cost GNSS receivers [24]–[26], but the instruments require integration of customized external components and are not ubiquitous. To bring this technique into the mass-market, we conjecture that smartphones (without any additional hardware) can be used as GNSS receivers through the use of their internal antennas and GNSS chipsets in order to perform remote sensing of the environment [27]. This article presents, to the best of authors' knowledge, the first published experimental demonstrations that reflected GNSS signals received via a smartphone device from a small UAS can be used to sense land features. This work has become possible thanks to direct access to raw GNSS data from mass-market devices running the Android Nougat (or newer) operating system, which was made available in 2016 [28].

We first discuss multiple experiments that were designed using a multicopter UAS platform, which has flown over water bodies and agricultural fields in late 2018. The purpose of the experiments was to observe the change in the reflected signal over land features (e.g., crop types, soil wetness) and transition from land to water. Two identical smartphones attached to ground plates (located on the top and bottom of the drone) are used to separate direct and reflected Global Positioning System (GPS) signals. Consistent with the results obtained by other recent airborne observations [14]–[16], a much stronger reflected signal has been observed over ponds and there has been appreciable spatial variations over lands. However, it has

Manuscript received July 13, 2020; revised November 15, 2020; accepted November 23, 2020. Date of publication November 27, 2020; date of current version January 6, 2021. This work was funded by USDA Agricultural Research Service(USDA-ARS), Award NACA 58-6064-9-007. (Corresponding author: Mehmet Kurum.)

The authors are with the Department of Electrical and Computer Engineering, Mississippi State University, Mississippi, MS 39762 USA (e-mail: kurum@ece.msstate.edu; mf1413@msstate.edu; gurbuz@ece.msstate.edu).

Digital Object Identifier 10.1109/JSTARS.2020.3041162

also been shown that the received signal power levels can be significantly modified by the orientation of smartphones due to the poor quality of the smartphone GNSS antenna, which can make the analysis of received signals challenging for remote sensing applications. To further examine the in-built antenna effects on the reflected GPS signals and the quality of GPS chipset used in smartphones as well as repeatability of the results, several follow-up experiments were carried out in 2020 [29]. First, the effect of antenna orientation (both elevation and azimuth) on the received signal is quantified using a pan/tilt equipment attached on a tripod for multiple days to see if the antenna radiation pattern is repeatable. Second, smartphone measurements are compared against a survey-grade custom-built GNSS receiver by flying them in separate multicopter drones over land and waters. Finally, the consistency of the reflected signals over both water and land is assessed by flying the UAS at different times of the day on two consecutive days.

The rest of this article is organized as follows. Section II describes the GNSS-R methodology applied to smartphones, experimental design, and characteristics of the study area. Section III presents and evaluates the experimental results. The implication of findings and the potential future application of smartphone-based GNSS-R approaches are discussed in Section IV. Finally, Section V summarizes this study.

II. MATERIALS AND METHODS

The GNSS signals received by smartphones include both the direct signal from satellites and multiple reflections from the surrounding area. The effects of multipath signals can be observed in the carrier-to-noise density ratio (C/N_0) and are considered as a source of error in the positioning, navigation, and timing studies. On the other hand, from a remote sensing perspective, the multipath signals offer great potential to understand the surrounding environment. For instance, the ground reflections (multipath) are intrinsically related to the soil moisture since the primary physical property that affects the L -band ground reflections is directly dependent on the amount of water present in the top 5-cm soil. However, separating direct and reflected signals is not a trivial task as they are highly convoluted with the smartphone's internal antenna properties and interfere with each other due to long chip length (e.g., about 300 m for L1 C/A signal).

Fig. 1 shows a proof-of-concept integration of smartphones into a multicopter small UAS. One smartphone (phone A) is placed to the upper disc of the UAS and pointing in the zenith direction (up-looking) while the other smartphone (phone B) is mounted on lower plate of the same UAS and pointing toward the nadir direction (down-looking). Both discs have 12 in (30.48 cm) in diameter and are made of acrylic plexiglass discs whose surface are covered by adhesive copper tape to block signals coming to the other sides of the discs. In order to minimize the effects of electronics/parts of the drone, the upper disc is mounted above the drone while the lower disc is placed below the drone when the drone legs are in the folded position. With this configuration, direct and reflected signals will be independently observable by phones A and B, respectively.

The point on which the reflected signal follows the shortest multipath is called the specular reflection point, where the incident and reflected waves make the same angle with the

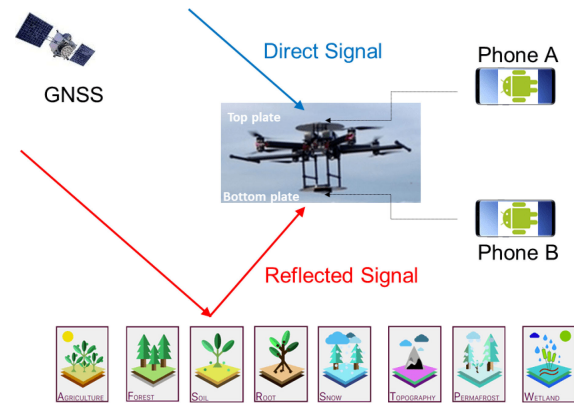


Fig. 1. Smartphone-based GNSS-R concept and arrangement of smartphones on the multicopter drone platform. Phone A (attached to upper plate) collects direct signals while phone B (attached to bottom plate) collects reflected signals. The reflected signal is expected to contain useful information on the surface.

surface normal. The specular reflection point is determined from simple image theory by confining the problem to a plane earth. Any other scattering around the specular point will follow longer path and is called diffuse scattering, which can be ignored in case of smooth soil and short vegetation [7], [9]. Depending on the terrain conditions, the specularly reflected signals acquired by phone B are expected to vary while the direct signals received by phone A are expected to remain unchanged under short-time periods and the same phone orientations. The reflected signal received by phone B can be then potentially utilized for a number of applications.

A. Description of the Initial Experiments

Three experiments, including a horizontal straight flight, a flight with changing altitude over pond, rotating flight at a fixed altitude, were designed and conducted on September 14 and 19, 2018, at The R. R. Foil Plant Science Research Center, known as North Farm at Mississippi State University. These experiments were carried out to investigate the possibility of land remote sensing using a smartphone internal antenna paired with in-built GNSS chips. The wind was a light breeze in both days while air temperature was roughly 30–32 °C. There was no rain during or between the experiments, but the ground was relatively wet due to a rainfall on September 13. The aerial picture of the site is shown in Fig. 2 and the lower left corner of the study area is located at 33° 28' 13.3" north and 88° 47' 18.7" west. North Farm is comprised of approximately 750 acres and includes tillable flat land with diverse agricultural crops. The study area contains two large water bodies as marked with blue boxes in Fig. 2: pond #1 (120 × 120 m) on the west side while pond #2 (80 × 120 m) in the east side.

- 1) *Horizontal straight flight*: In the first experiment (September 14), the drone was flown autonomously at a fixed altitude (15 m) with 5 m/s ground speed along a straight path from points A to B and followed this same path back to point A. The distance between points A and B was roughly 1.5 km and the total round trip flight time during this scan was 9 min 39 s. The ground track of the flight is shown with a red line (between points A and B) in Fig. 2 and passes over various croplands (i.e., soybeans, rice,



Fig. 2. Upper panel: An aerial picture (credit: Google Earth) of study area with crop types, overlaid and differentiated with color. Lower panels from left to right: Pictures from soybeans, rice, corn, and cotton fields, respectively, taken on September 14, 2018. Ground specular reflection track associated with PRN #12 satellite during the first experiment is overlaid with the aerial image and colorized with C/N_0 (blue being the highest and yellow being the lowest signal strength).

corn, and cotton), unpaved roads, ditches, grasslands (in between fields and roads), and two ponds. The purpose of this experiment was to observe the change in the reflected signal over land features (e.g., crop types, soil wetness) and transition from land to water as depicted in the upper left panel of Fig. 3.

- 2) *Changing altitude over pond:* In the second experiment (performed immediately after the first experiment), the altitude of the drone was changed in continuous and incremental modes in the middle of the pond #1 (the point C in Fig. 2), and the procedure took 9 min 55 s to complete. In the continuous mode, the altitude was manually increased from 5 to 50 m at a slow pace, and then decreased from 50 to 5 m at a similar pace whereas in the discrete mode, the altitude was increased with 5 m increments (staying at each height roughly one minute) back to 50 m. As depicted in the bottom panels of Fig. 3, the specular reflection points move out or in when the drone ascends or descends, respectively. This experiment is another way to achieve land/water transition when the drone is over a water body.
- 3) *Rotating at a fixed altitude:* The last experiment (September 19) took place over a uniform grass field (the point D in Fig. 2) to further investigate the effect of antenna pattern on the received signal. The typical antennas used in smart devices are designed to be omnidirectional and

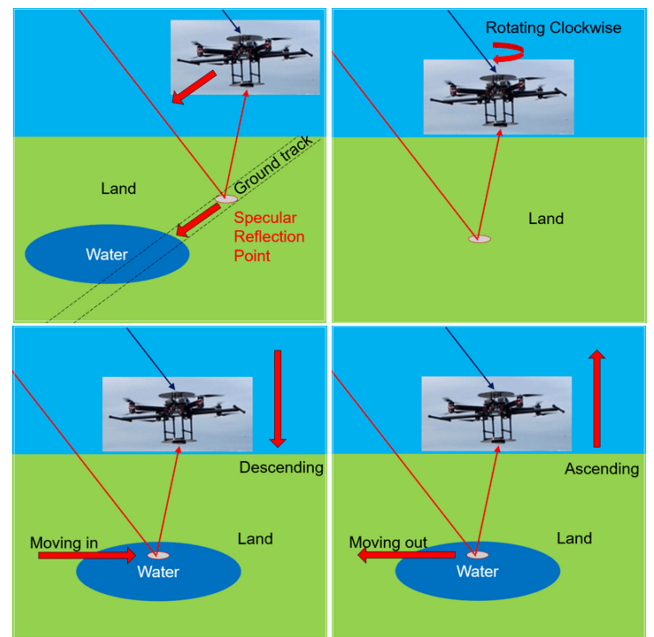


Fig. 3. Experimental strategies: Straight flight over land/water (upper left), changing altitude over water (lower panels), and rotating at a fixed altitude over a uniform land (upper right).

linearly polarized, but their pattern can be irregular or distorted due to design and placement requirements within the smartphone along with other electronic circuits [30]. To receive the signals through the antennas at different azimuthal directions, the drone is (1) rotated clockwise in azimuth at a fixed altitude (10 m), starting from north back to north with 45° increments (staying at each azimuth location roughly one minute), and (2) continuously rotated three-times covering full azimuth rotation. This experiment took roughly 11 min and 21 s.

In these experiments, two identical smartphones running the Android Oreo operating system (Samsung Galaxy S9) was utilized. GPS raw data were collected and stored in receiver independent exchange format (RINEX) format with a one-second sampling rate by using an Android app called rinexON, which is freely available at Google Play store. Due to the duty cycle of the GNSS chip's primary oscillator, the raw data acquisition takes around 200 ms for every second [31]. The app provides average values every seconds. In order to document the experiments, the front cameras of smartphones are turned on and the entire experiment was videotaped using a background video recorder Android app. The timing of each important event such as starting/ending of a procedure, passing over a pond or cropland, changing altitude, and rotating the drone, were identified from these video records.

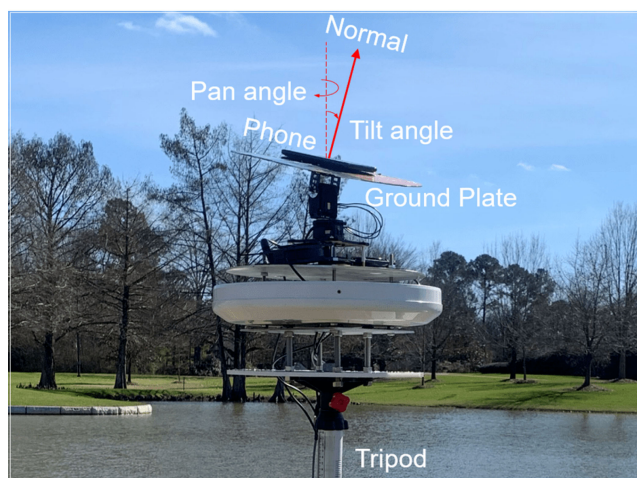
The aforementioned experiments were conducted between 17:30 and 18:15 in Coordinated Universal Time (UTC) time on each day to observe the same GPS satellites at similar positions in the sky. Since the orbital period of GPS satellites is 12 sidereal hours, the positions of GPS satellites in sky change several degrees during the flights. The smartphone GNSS receiver can acquire multiple GNSS signals simultaneously. During these experiments, 9–10 satellites were visible, but most of the data were not useful for this analysis. For instance, the signals from the Pseudo random noise (PRN) code #6, #9, #13, and #19 were much more noisy and there were some data interruptions for these satellites since the elevation angles were lower than 20° , which can be affected by multipath significantly (as we clearly observed in the follow-up experiments). In addition, the phone did not collect signals from PRN #2 and #5 (elevations $> 60^\circ$). The reason is not apparent to us, but the same issue repeated for future experiments consistently. The remaining “quality” data come from PRNs #12, #25, and #29 GPS satellites where their mean elevation angles are 39.3° , 39.6° , and 28.7° , respectively. Among these, the specular points from PRN #29 fell out of ponds so we could not observe the land/water transition. As a result, the results of the initial experiments are limited to the observations from PRN #12 GPS satellite only. While this seems a limitation in analysis, we address the repeatability of the measurements in the follow-up experiments.

B. Description of the Follow-Up Experiments

As presented in following section, the results of the initial experiments demonstrated that the received signal strength varied significantly by the orientation of smartphone [as the drone changes orientation (roll, pitch, and course) during the turns], owing to the poor quality of the smartphone's inbuilt antenna (dips/nulls in the pattern). In order to provide further insights



(a)



(b)

Fig. 4. Small UASs and pan-tilt configurations. Top: a mid-size quadcopter with smartphone attached to a gimbal and a large octocopter with a custom GNSS-R system. Bottom: a pan-tilt setup to measure GNSS signals via a smartphone in various elevation and azimuth orientations.

on the quality of both in-built chip and antenna of a smartphone with regard to the GNSS-R approach as well as consistency of measurements, several follow-up experiments were conducted. These include a pan-tilt experiment and a formation flight as described in the following.

- 1) *Pan-tilt experiment*: A smartphone is attached in the middle of a ground plate that is the same one used in the initial experiments (a 12 in acrylic Plexiglas discs with adhesive copper tape on its surface). This arrangement is mounted in a face-up orientation on a pan-tilt kit, placed on a tripod to freely rotate the smartphone in both elevation and azimuth directions as shown in Fig. 4(c). The tilt angle varied from 0° (zenith direction) to 20° with 2° increments over full 360° azimuth rotation (pan angles) at each increment to cover a typical drone orientation changes (roll, pitch, and course) in the previous experiments. In azimuth direction, it takes 36 s to complete 360° degree. In the next second, it changes the tilt angle and starts rotating in the opposite direction to complete 360°

in azimuth. This process repeats until all tilt angles are finished. One complete cycle takes $408 (= 37 \times 11 + 1)$ s. The same cycle continuously repeated 35 times (approximately 4 h) to observe GPS signals at various satellite elevation angles. Two identical phones (Phones C and D) are utilized at multiple days (two days for each phone in alternating order) to check if the data are consistent over different days and across phones of the same model. The experiments took place in an open area on campus on January 22, January 25, January 28, and February 14, 2020. The start time of upcoming measurements shifted accordingly as the same satellite configuration is repeated 4 min earlier every day for one and the same location due to the sidereal revolution period of the GPS satellites (11 h 58 min).

2) *Formation flight*: This experiment involves flying two UASs (a mid-size quad-copter and a large-size octo-copter) in close proximity in time (about 20 s apart) autonomously at a fixed altitude (15 m) with 5 m/s ground speed along the same flight path on February 3, 2020. The octo-copter carried a high-end dual channel GNSS-R system as shown in Fig. 4(b), the quad-copter carried a smartphone that is attached to a gimbal, as shown in Fig. 4(a). This setup is aimed for both receivers to acquire the reflected signals over the approximately same Fresnel zone at nearly same GPS transmitter observation angles. Fig. 2 shows the ground tracks (colored as a black line) of the formation flight that start at the point E, turn around the segment F and end at the point G. The flight plans were designed so that the drones pass over pond #2 and the course of both drones is fixed in one direction during entire flights (facing clockwise 1° from north aligned with the row structure of the farm in the south of the pond). The flight data (barometric altitude with respect to the sea level, heading, pitch, and roll) from both drones are compared and it is observed that the pitch and roll angles vary $\sim 10^\circ$ and $\sim 15^\circ$, respectively, when the drone turns between times t_2 and t_3 (the segment F in the figure) while they are relatively stable (within $\sim 3^\circ$) and $\sim 10^\circ$ offset in pitch angle for each direction for the remainder of the time (during the straight paths). The changes in barometric altitude are not expected to be precise and varied (~ 3 m) even over ponds when the flight passes over as highlighted with blue.

3) *Repeated flights*: The purpose of this experiment is to check the consistency of the reflected signals over both water and land by flying the UAS at different times of the day on two consecutive days. The same flight configuration in the previous flight (formation flight) was employed to the mid-size quad-copter carried a smartphone that is attached to a gimbal, as shown in Fig. 4. On the first day (June 6), the experiment started at 14:24, 18:06, and 19:23 UTC time while the next day, the same flights were repeated 4 min. earlier. There was no rain between these measurements so the ground conditions could be assumed to be relatively similar.

In these experiments, two dual-frequency GNSS smartphones were used to acquire C/N_0 at L1 ($= 1575.45$ MHz) and

L5 ($= 1176.45$ MHz) frequency bands from multiple GNSS constellations including GPS, Galileo, GLONASS, and Beidou satellite transmissions. The GPS L1 data were used only and recorded in RINEX format with a one-second sampling rate by using the rinexON Android app to be consistent with our initial experiments, which were done with Samsung Galaxy S9 (L1 GPS chips only) in 2018. While feasibility of L5 frequency band remains to be studied, we expect similar frequency response due to close proximity of L1 and L5 bands but improved noise performance for L5 signals since L5 has a faster chipping rate, making the main peak in the autocorrelation function sharper compared to L1 signal acquisition.

For the formation flight, one smartphone is mounted on a circular mesh at the bottom of the quad-copter in the nadir direction (down-looking). In order to minimize the effects of smartphone orientation during the drone turns and the flights in opposite directions, a gimbal is placed below the drone. After several trials of ground plates, a chicken wire mesh with gaps smaller than one-tenth of a wavelength was found the most optimal as it helps to reduce the airflow and, thus, ease the aerodynamic drag on the gimbal.

The high-end dual channel GNSS receiver is a commercial software-defined radio that provides synchronized GNSS IF sample data streams from two separate antennas. A standard right-hand circularly polarized (RHCP) antenna is mounted on a ground plate above the drone to receive direct signal while an omnidirectional (hemispherical with 114° 3 dB beamwidth in free space) left-hand circularly polarized antenna is mounted on a ground plate below the drone to capture reflected signal. The ground plates are fixed to the drone frame and made of 12 in acrylic plexiglass discs whose surface are covered by adhesive copper tape. The receiver correlates the received signals with a clean replica of the L1 C/A code to calculate the peak correlation value referenced to the noise level, the C/N_0 , tracking, and other observables in postprocessing. In the beginning of each experiment, a calibration routine is performed where the direct antenna is connected to both channels with power divider to crosscalibrate the gain and line discrepancies between the up- and down-looking paths. The signal acquisition and tracking computations are performed using raw data acquired by the direct signal channel while a master-slave scheme (using tracking parameters from the direct signal) is utilized to process the reflected signals offline. This receiver is considered as a reference and used to evaluate the performance of smartphone GNSS chipset by flying in formation as described earlier.

III. RESULTS

In this section, the direct and reflected data from GPS signals from the three initial experiments are first provided and discussed. Then, the results of the follow-up experiments are presented and discussed.

A. Results of the Initial Experiments

The results of the initial experiments are limited to the observations from PRN #12 GPS satellite only. The position of the PRN #12 GPS satellite varied roughly from 40° to 30° in elevation and from 200° to 210° in azimuth during the time

periods that cover three experiments. Fig. 5 shows the temporal trends of acquired C/N_0 data for each experiment. In all plots, the blue dots represent data collected by Phone A (direct signal) while the red dots denote phone B (reflected signal).

In the first experiment, the drone flies toward east from time t_5 to t_{10} as indicated in Fig. 5(a). While it transitions from land to the first pond (transparent blue shaded area) at t_6 , the reflected signal jumps about 8 dB, remains at a similar magnitude while over the pond, and then drops about 8 dB again at t_7 when it reaches the land again. Similar behavior is also clearly seen when the drone passes over the second pond (which is narrower in east–west axis). While the reflected signal strength stays relatively stable over both ponds, the same plot also shows that the fluctuation (difference of maximum and minimum) over land is rather large (around 8 dB, the average standard deviation is close to 2 dB). To further explore the cause of these large spatial variations over land, the C/N_0 data for this time frame (flying east) is also overlaid with the aerial image, showing crop field boundaries, roads, and ponds in Fig. 2, where blue color indicates high reflections and yellow color denotes lower reflections.

There are some remarkable spatial features associated with the C/N_0 fluctuations over land as seen in Fig. 2. In the beginning of the flight (starting from point A), the specular points that reside on the unpaved road (which was dryer than the crops fields) show lower C/N_0 values (yellow color), consistent with the other road crosses of the specular tracks later in the flight. The reflected signal then increases and stays high (light blue) over soybeans since it was relatively wet and covered with light vegetation. The signal strength decreases again when the drone is over rice field which had similar soil conditions but was covered denser vegetation amount than soybeans. This difference can be attributed to the foliage attenuation of dense rice plants. The signal strength right before and after both ponds shows the lowest values (bright yellow) since the surrounding area around the ponds are covered by mowed short grass on relatively dry steep slope, which kept them relatively dryer. The C/N_0 stayed relatively high over corn fields since the soil was wet and corn was in the late senescence stage (light vegetation). The signal strength over the cotton field near the second pond exhibits an interesting pattern [alternating low (yellow) and high (blue) reflectivity values]. This periodic fluctuation is highly correlated with the cotton field pattern, which is aligned along north–south strips (roughly 5-m wide bare soil space between 15-m wide cotton fields of 9 total strips) as confirmed with the phone video recordings. Last but not least, in the close-up pictures on Google Earth and the video taken by the phone’s front camera, the signal strengths can be easily distinguished between the dry roads and wet ditches around the roads.

The qualitative analysis of the high jump in the reflected signal power over both ponds and spatial variations over land indicates that the fluctuations over land carry information in addition to noise and they are due to the change in crop types, roughness, and moisture in the soil. These results are consistent with resent experimental results [14]–[16] and support the assertion that reflected signals collected by smartphones are highly sensitive to water content on the surface, with similar dynamic range observed by regular custom-built GNSS-R instruments. However,

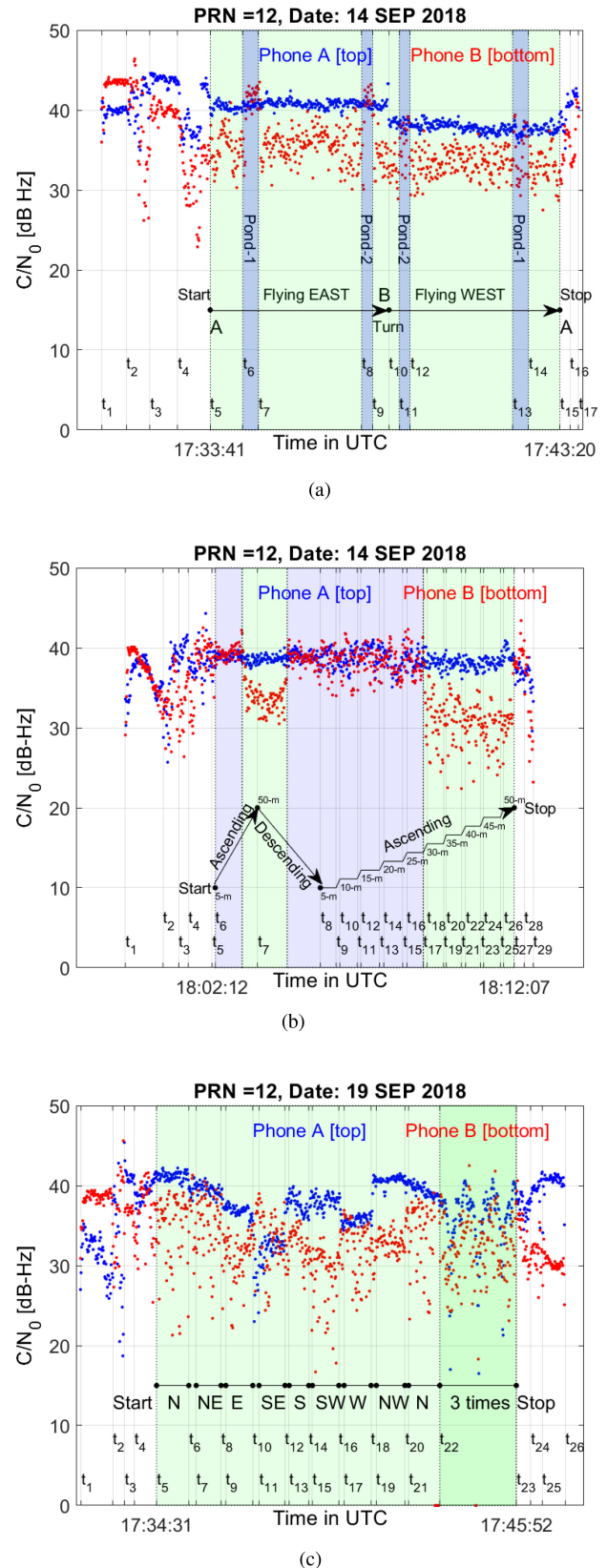


Fig. 5. Experimental results of GNSS-R received power over (a) horizontal flight track over ponds and crops, (b) vertical flight depicting the movement of a specular point over land and water, and (c) azimuth rotation depicting smartphone antenna pattern irregularities.

it is necessary to have detailed *in situ* data in conjunction with experimental data in order to quantitatively verify the results.

Also, as seen in Fig. 5(a), the direct signal (Phone A) stayed almost constant and carried less fluctuations (standard deviation is less than 0.5 dB) from t_5 to t_{10} as was expected. However, the direct signal strength was lower than the reflected signal (Phone B) over ponds when flying toward east, and the direct and reflected signal strengths drop about 2–3 dB on average after the drone turns back at point B at time t_{10} (180° change in drone heading). Both of these observations can be attributed to the irregularity of the in-built antenna's radiation pattern since relative antenna orientations of both phones are mirror image of each other so the opposite side of the smartphone antennas sees the same satellites. In other words, both phones are identical and are placed on identical ground plates. However, phone A is facing up while the phone B is facing down. This means that when the drone was flying east, the right (left) side of the phone B (phone A) was facing south, where PRN#12 satellite is located. Since Phones A and B are looking at opposite sides and the phone electronics are not symmetric with respect to its center, they see the satellites with different angles, and hence, the antenna gains for the direct and reflected signals could possibly be different due to irregular antenna patterns, leading a higher reflection power in Phone B than what phone A receives as the direct signal. In addition, the reflected signals (Phone B) over the ponds on the way back (flying west) also show an increase compared to land which are not as strong and stable as those when flying east. This is again due most likely to the irregular antenna pattern.

In the second experiment as shown in Fig. 5(b), the drone starts ascending from 5 m at t_6 and arrives 50 m at t_7 in the middle of pond #1. The reflected signal stays high for a while and then drops suddenly (about 8 dB) before reaching the 50 m. This is because the specular points move out of the pond as depicted in Fig. 3. After arriving at 50 m, the drone starts descending gradually until it arrives at 5 m at t_8 . As clearly seen from the plot, after a certain altitude, the reflected signal jumps back to the high values (8 dB increase). In this case, the specular reflection point moved into the pond as it descends. From t_8 to t_{26} , the drone starts to ascend again, but this time incrementally. At each 5-m increments, it stays at that position for about 1 min. Finally, the drone arrives at 50 m. As clearly seen, somewhere between 25 and 30 m, the specular point moves out to the land. These values are in close agreement with specular point calculations using satellite position, although analysis could be slightly inaccurate due to errors in GPS elevation angles and accurate drone height and position measurements. The reflected signals drop about 8 dB again as the specular point moves out of pond. The segment between t_8 and t_{26} shows more fluctuations than the segment between t_6 and t_7 as the incremental altitude change (t_8 to t_{26}) added more effort to stabilize the drone orientation in which the drone did not have any stable gimbal system. Therefore, the orientation of phone was more variable for the incremental mode, which made antenna effects more apparent in the data. Nonetheless, a similar significant contrast between the land and water regions can be observed in this time frame as well. The higher fluctuations are due most likely to antenna effects whose pattern is expected to vary across various orientations.

Both experiments confirm the sensitivity to the water/land transition via reflected signal acquired by smartphone GNSS

receivers. However, both experiments also indicate that the antenna pattern plays an important role in the strength of received signals. To further observe the effect of smartphone orientation on the received signal, a third experiment was conducted. The results are shown in Fig. 5(c). From t_5 to t_{22} , the drone azimuth orientation changed 45° clockwise and the drone stayed at each discrete direction about one minute starting from north and covering full azimuth plane. At t_{22} , the drone started to rotate continuously three times until t_{23} . As clearly seen in both segments (t_5 to t_{22} and t_{22} to t_{23}), the direct signal (as well as the reflected signal) strength varies significantly, close to 10–15 dB. Since the measurement periods are relatively short (particularly the second segment), one can assume that incoming GPS signals stayed approximately the same. Thus, it is evident that the in-built antenna radiation pattern is highly irregular and highly depends on smartphone orientation.

B. Results of the Follow-Up Experiments

The data presented in the previous section provided encouraging results with visual confirmation of the correlation between spatial fluctuations of moving GNSS specular reflections and ground features such as land/water transition, crop types, and soil conditions. The results also indicated that the poor quality of in-built GNSS antennas is the main pitfall in use of GNSS-R techniques from smartphones. Furthermore, as the changes (fluctuations) in the signal strength over land were rather large (about 8 dB from minimum to maximum), the question remains if the reflected signals remain consistent at different times. This necessitated conducting further experiments to quantify and to provide further insights on the quality of both in-built chip and antenna of a smartphone with regard to the GNSS-R approach as well as the consistency of the data under the same configuration.

In Fig. 6, direct C/N_0 measurements by the smartphones C and D on a tripod with a pan-tilt mechanism are shown over a period of approximately four hours with the same configuration in four different days. The results are given for PRN #8 satellite (similar results are obtained for other PRNs but not shown here). Each subplot shows the data for phone C (phone D) in every second intervals and one-minute running averages in blue and red (red and blue) colors, respectively, while the elevation and azimuth angles (given in the right axis) are provided in black dashed line and green dash-dotted line, respectively. The elevation angle shows a large dynamic range (from 0° to $\sim 75^\circ$) for this time frame. Early fringes in the C/N_0 arcs, up to about 40° elevation, is due to ground reflection multipath. Based on the visual comparison of these plots at higher elevation angles (larger than 40°), it is evident that the measured data demonstrate a similar and consistent pattern for each day.

To quantify the correlation between each measurement set, the covariance matrix is calculated and off-diagonal elements, which result in six unique pairs (cross correlation) from four measurements, are provided for each cycle in Fig. 7. While the upper panel shows correlation coefficients (R^2) of mean (solid line) and individual (dots) pairs, the lower panel shows root measure square error (RMSE) of mean (solid line) and individual (dots) pairs for each cycle. The red lines and dots denote the results from the pairing of individual measurements while the

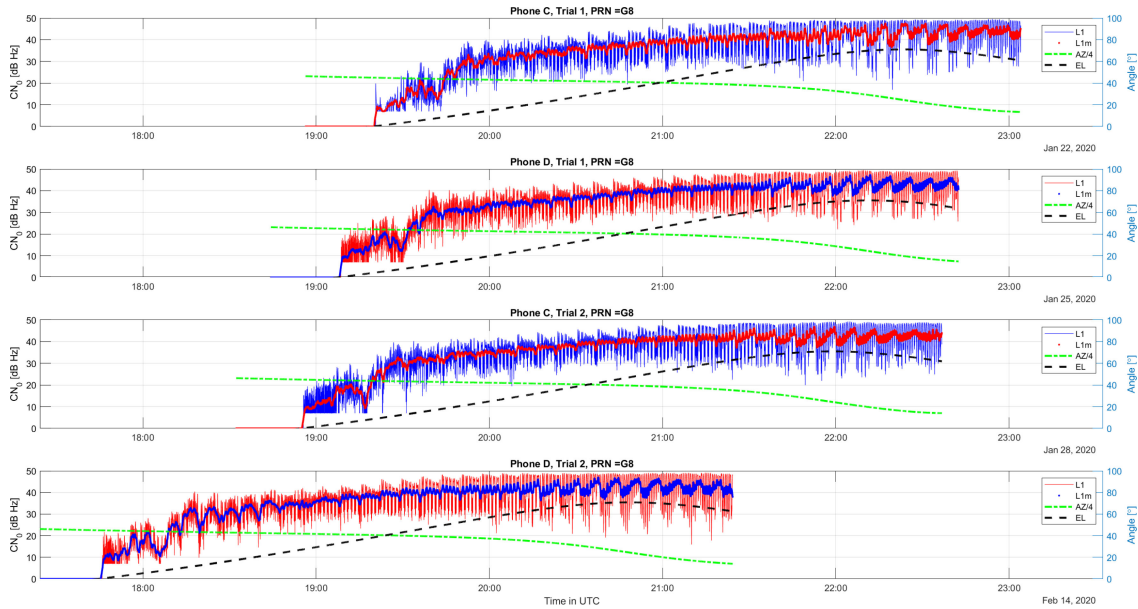


Fig. 6. Temporal trends of the pan-tilt data set that covers approximately four hours (34 cycles) by two separate smartphones in four different days (in the order of phones C, D, C, and D from top to bottom).

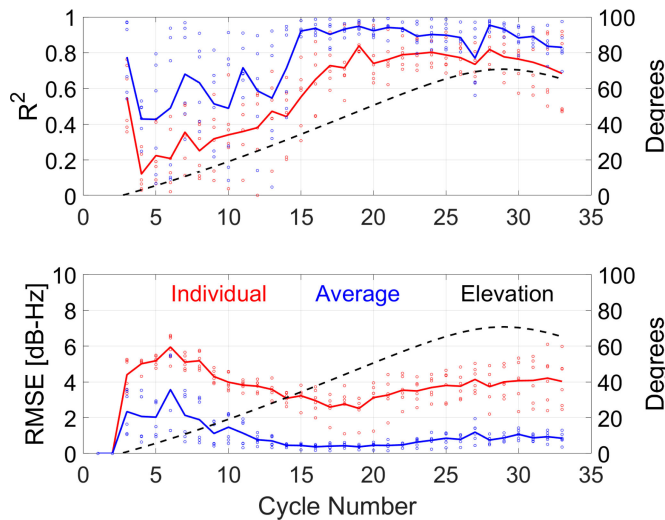


Fig. 7. Correlation coefficients and RMSEs of pairs of the pan-tilt dataset for PRN #8 in different days as a function of cycle.

blue lines and dots represent the results from the pairing of a one-minute running average of measurements. The elevation angle (dashed lines) is also given in the right axis to interpret results as a function of angle. The results show that the measurements across different phones and times are highly correlated with each other and the RMSE is relatively low for higher elevation angles (more than 40°) under the same configuration. As expected, the correlations and RMSEs are quite poor for lower elevation angles due to the increasing multipath contributions. This experiment illustrates the time-invariant nature of the pattern over different days and across different phones of the same model at high elevation angles. It is, thus, possible to characterize the antenna

pattern effects as a look-up table ahead of time and to compensate its effects for given orientation during the flights.

To illustrate the angular behavior of the C/N_0 data on the phone orientation, measurements by the phone C in the first day are plotted in a polar format for three cycles in Fig. 8. The plot is divided into 11 concentric circles to represent each tilt angle. In each concentric circles full azimuth scan is provided, where the size of circles gets larger with the tilt angle. This close-up plot illustrates a high variability (~ 20 dB) of C/N_0 as a function of the phone orientation even though the satellite elevation and azimuth angles remain relatively constant over one cycle (418 s). The results at higher elevation angles show relatively uniform signal strengths and variations are due mostly to change in the pan angles. The dips in certain azimuth orientations are also evident higher elevation angles. On the other hand, the variation in signal strength at the lower angles depend highly on both tilt and pan angles. It might be difficult to characterize the antenna at lower elevation angles due to the multipath contributions.

Next, Fig. 9 compares the reflected C/N_0 data collected by the gimbal-smartphone configuration [see Fig. 4(a)] against those acquired by the high-end receiver [see Fig. 4(b)] during the formation flight, where each of them was flown in close proximity in time over the same flight mission. Both reflected C/N_0 measurements from satellite PRN #8 are normalized by their maximum and shown in every second intervals and averages with eight seconds of moving windows as a function of the flight time in Fig. 9(a). The red circles and black lines indicate individual and average smartphone C/N_0 measurements, respectively, while the red asterisks and blue lines denote individual and average custom receiver C/N_0 acquisitions, respectively. The flight tracks, which are overlaid with a recent background image, are shown in Fig. 10. Also shown in the figure is the smartphone C/N_0 data projected on the first Fresnel zones, based on the geometric configuration of satellite and the drone. There are

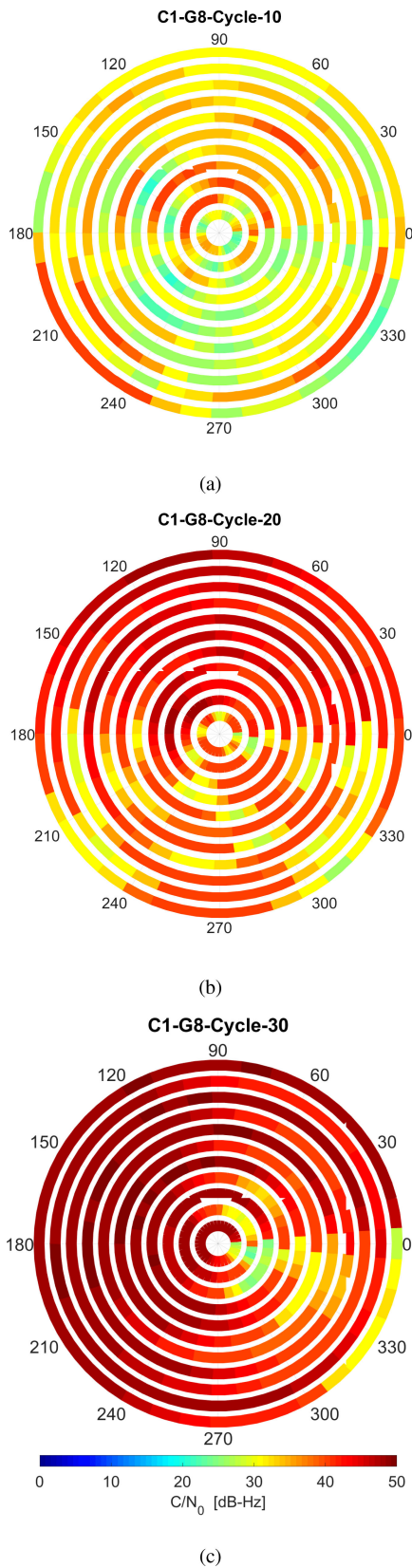


Fig. 8. Examples of complete cycles of the pan-tilt data set are shown in polar coordinates. The data at Cycles # 10, 20, and 30 (from left to right) are acquired at elevation angles of approximately 20°, 50°, and 70°, respectively.

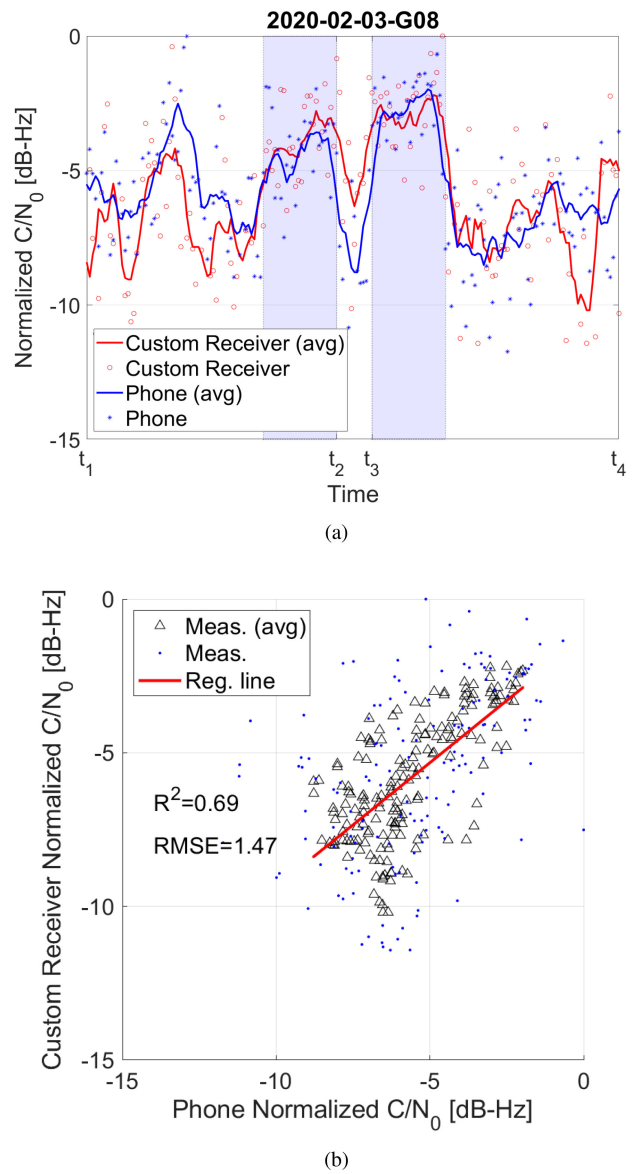


Fig. 9. Formation flight data acquired by a survey-grade GNSS-R receiver and a smartphone are shown in (a) temporal and (b) scatter plots.

two flight lines in the north–south direction (red arrows show the flight direction along each line) and the drones pass the pond #2 twice in opposite directions. The time frames, where the drones pass over the pond, are highlighted with the blue shaded area in Fig. 9(a). The response from water is apparent in both datasets. When the specular ground points transition from land to the pond, the reflected signal shows a clear jump and remains at a similar magnitude with some variations while over the pond, and then drops and shows variations again when it reaches the land again. For instance, both data show a strong reflection over the field in the first flight line where the drones fly north. Surprisingly, the smartphone data showed higher values (dark blue ellipses in Fig. 10) than those over the pond. It is most likely due to the saturated soil (particularly wet area within the field). Due to inaccuracies in the flight data as a result in variability of the altitudes, it is not expected to have a perfect match over land.



Fig. 10. Flight path (red line) and the smartphone's ground specular reflection tracks associated with PRN #8 satellite are overlaid with the aerial image and colored with C/N_0 (blue being the highest and yellow being the lowest signal strength).

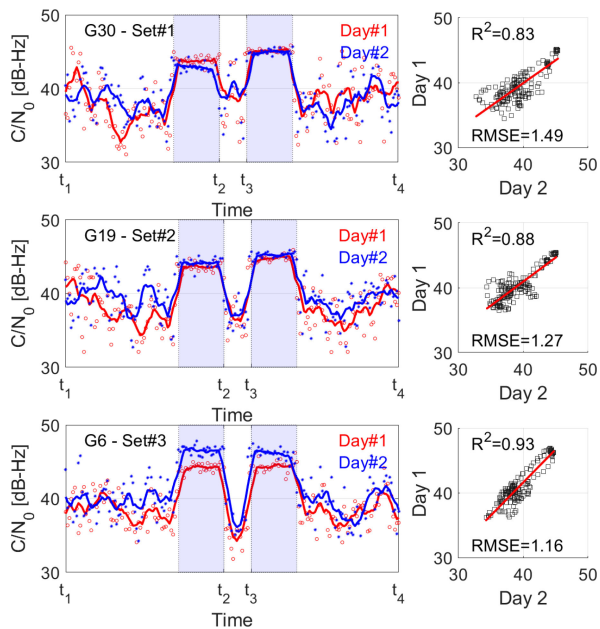


Fig. 11. Smartphone data acquisition using the mid-size quad-copter gimbal system three different time frames on two consecutive days.

Nonetheless, the C/N_0 values show a similar trend and dynamic range in both cases. Fig. 9(b) provides scatter plot where data are provided in individual measurements and averages with eight seconds of moving windows. The correlation coefficient of 0.69 and RMSE of 1.47 dB-Hz demonstrate a moderate to strong linear relationship. A stronger relationship would be obtained if the higher position accuracy between formation flights were achieved by utilizing the GNSS real-time kinematic system. The high correlation indicates that the smartphone's internal GNSS chip produces C/N_0 of similar quality compared with a survey-grade receiver.

In Fig. 11, the reflected signals are compared over the same north-south flight path given in Fig. 10 in order to check if the

larger changes (fluctuations) in the signal strength are consistent under the same configuration at different times of the day on two consecutive days. The smartphone data acquisition is done using the mid-size quad-copter gimbal system as described earlier to keep the phone heading the same for the entire flight duration. In particular, three different time frames and various PRN satellites are chosen to show that the results are consistent over various high elevation angles (i.e., 53° , 59° , and 77° for PRN #30, 19, and 6, respectively). The time frames, where the drones pass over the pond, are highlighted with blue shaded area in the figure. While the left panels show the eight-second moving average (solid line) and individual (dots) signal strengths (C/N_0) at each seconds of measurement, the right panels show corresponding scatter plots and correlation metrics. The correlation coefficients of 0.83, 0.86, and 0.93 and RMSEs of 1.49, 1.27, and 1.16 dB-Hz were achieved, which demonstrate strong linear relationships between consecutive days for each set. Furthermore, the signal strength levels remained above 30 dB-Hz, which is within the signal strength ranges where the most GPS receivers can maintain the lock. The repeatability of the experiments also supported that the phones continued to operate satisfactorily without loss of signal tracking. This indicate that high variability of signals strength (particularly over land) is due to the spatial features on the ground.

IV. DISCUSSION

This study explores the possibility of remote sensing of soil moisture using mass-market platforms (smartphones and drones). It is clear that smartphone is not designed for such tasks and needs improvement in hardware or processing approach. We designed several experiments to demonstrate if it is possible to process smartphone data (without any custom hardware) in conjunction with a small UAS to sense water in soil. The success of the studies like this one has a significant implications as they can influence the agriculture economy, ushering in a host of precision irrigation applications that have so far been hampered by the cost and scarcity of custom-built instruments

in traditional GNSS-R. Raw GNSS measurements by mobile phones have been recently made available with the aim to open the door for new innovative ideas for using these measurements in mobile applications [28]. Most of the studies have been so far leaning toward the development of practical solutions to improve positioning techniques [31]. In this article, we took a novel approach that proposed the integration of smartphones into small UAS for the purpose of remote sensing. This approach has been inspired by developments in GNSS-R techniques where the GNSS satellite is being used opportunistically. Rather than developing a custom receiver that is not readily available and usually built in house, we used in-built GNSS chipsets in smartphones to detect and record reflected GNSS satellite signals. A proof of concept experiment has been designed and conducted to confirm some of already known properties of GNSS-R by using a mass-market smart device rather than a study into the development of a new GNSS-R technique. Reflected signals showed high correlation with spatial features on the ground. Similar and various other configurations can be further exploited since more experiments can be easily done with smartphone devices, which are inexpensive, easily accessible, yet powerful.

The main pitfall in using a smartphone as a passive radar receiver for the purpose of remote sensing was its poor quality of GNSS antennas. The irregular antenna pattern adds another complexity to readily available challenges within GNSS-R approaches such as quantification of surface roughness, vegetation, soil moisture for geophysical parameter retrieval. Antenna polarization crosstalk, and mismatch can greatly affect the performance of GNSS-R techniques. In addition, direct signal can have impact on the received reflected signal due to the long pulse width of L1 C/A code and antenna irregularities at particularly lower elevation angles. The follow-up experiments demonstrated that the radiation pattern of the smartphone's GNSS antenna are observed to be highly irregular, but time-invariant higher elevation angles. In other words, smartphone-grade antennas can be characterized by "quantitative" analysis. The smartphones are equipped with a plethora of inexpensive yet powerful embedded sensors such as a gyroscope and camera. It could be possible to correct the antenna pattern if true orientation of the smartphone is predicted via its embedded sensors. Furthermore, it was shown that the smartphone's internal GNSS chip produces C/N_0 of similar quality compared with a survey-grade receiver.

The results presented in this article should be considered preliminary, which did not intend to resolve all of these issues. We rather aimed to provide an initial assessment of the potentiality of this ubiquitous technology along with its shortcomings and to bring it in the attention of GNSS-R community so that we as the research community can start investigation solutions to possible causes/challenges. Even though smartphone-based GNSS-R will never be expected to outperform high-end GNSS-R instruments unless the quality of the in-built antenna is improved, nonetheless, this is a promising research avenue to investigate how far smartphones can take us. For instance, with the possibility of acquisition of up-to-date and fine-grained soil moisture information through mass-market smartphone devices and the availability of such information to individual users, we envision that sharing such information through mobile crowd sensing could greatly contribute to not only field scale applications

but also large scale applications within the hydrological and atmospheric studies.

V. CONCLUSION

This study presented the first experimental evidence of the use of a smartphone in-built GNSS sensor as a multistatic radar receiver for the purpose of land remote sensing. The reflected signal showed consistent spatial correlations with surface features, including high reflectivity over ponds, sensitivity to land crop types and moisture in the soil, consistent with the previous GNSS-R experiments with custom-built equipment. The contrast between water ponds and agricultural fields is relatively easy to be measured. However, the reflectivity of crop fields is complicated by many more unknown variables within the measurement scene as the soil contribution can be suppressed by a combination of effects from vegetation, tillage, surface roughness, soil type. The received signal power levels can also be significantly modified by the orientation of smartphone due to irregular radiation pattern of its GNSS antenna, but it could be possible to characterize the antenna pattern effects as a look-up table ahead of time and to compensate its effects for given orientation during the flights since it was found that the radiation pattern was time-invariant over different days and across different phones of the same model. Furthermore, the internal GNSS chip produces observables of sufficient quality when the GNSS smartphone reflected signals are compared with a high quality custom-built dual channel receiver. Ultimately, in order to truly reach to the mass-market, one needs to 1) define a calibration scheme that factors antenna effects out, and 2) quantify contributing geophysical parameters (vegetation, roughness, and moisture). This could be achieved via perhaps data-driven machine learning approaches backed with physics-based ancillary data.

REFERENCES

- [1] C. Hall and R. Cordey, "Multistatic scatterometry," in *Proc. Int. Geosci. Remote Sens. Symp., 'Remote Sens.: Moving Toward 21st Century'*, 1988, vol. 1, pp. 561–562.
- [2] M. Martin-Neira *et al.*, "A passive reflectometry and interferometry system (PARIS): Application to ocean altimetry," *ESA J.*, vol. 17, no. 4, pp. 331–355, 1993.
- [3] V. U. Zavorotny, S. Gleason, E. Cardellach, and A. Camps, "Tutorial on remote sensing using GNSS bistatic radar of opportunity," *IEEE Geosci. Remote Sens. Mag.*, vol. 2, no. 4, pp. 8–45, Dec. 2014.
- [4] J. L. Garrison, A. Komjathy, V. U. Zavorotny, and S. J. Katzberg, "Wind speed measurement using forward scattered GPS signals," *IEEE Trans. Geosci. Remote Sens.*, vol. 40, no. 1, pp. 50–65, Jan. 2002.
- [5] E. Cardellach, F. Fabra, O. Nogués-Correig, S. Oliveras, S. Ribó, and A. Rius, "GNSS-R ground-based and airborne campaigns for ocean, land, ice, and snow techniques: Application to the gold-RTR data sets," *Radio Sci.*, vol. 46, no. 6, pp. 1–16, 2011.
- [6] D. Masters, P. Axelrad, and S. Katzberg, "Initial results of land-reflected GPS bistatic radar measurements in SMEX02," *Remote Sens. Environ.*, vol. 92, no. 4, pp. 507–520, 2004.
- [7] K. M. Larson, J. J. Braun, E. E. Small, V. U. Zavorotny, E. D. Gutmann, and A. L. Bilich, "GPS multipath and its relation to near-surface soil moisture content," *IEEE J. Sel. Top. Appl. Earth Observ. Remote Sens.*, vol. 3, no. 1, pp. 91–99, Mar. 2009.
- [8] A. Egido *et al.*, "Airborne GNSS-R polarimetric measurements for soil moisture and above-ground biomass estimation," *IEEE J. Sel. Top. Appl. Earth Observ. Remote Sens.*, vol. 7, no. 5, pp. 1522–1532, May 2014.
- [9] N. Rodríguez-Alvarez *et al.*, "Land geophysical parameters retrieval using the interference pattern GNSS-R technique," *IEEE Trans. Geosci. Remote Sens.*, vol. 49, no. 1, pp. 71–84, Jan. 2011.

- [10] Y. Pei, R. Notarpietro, P. Savi, M. Cucca, and F. Dovis, "A fully software global navigation satellite system reflectometry (GNSS-R) receiver for soil monitoring," *Int. J. Remote Sens.*, vol. 35, no. 6, pp. 2378–2391, 2014.
- [11] A. Egido *et al.*, "Global navigation satellite systems reflectometry as a remote sensing tool for agriculture," *Remote Sens.*, vol. 4, no. 8, pp. 2356–2372, 2012.
- [12] H. Carreno-Luengo, A. Camps, J. Querol, and G. Forte, "First results of a GNSS-R experiment from a stratospheric balloon over boreal forests," *IEEE Trans. Geosci. Remote Sens.*, vol. 54, no. 5, pp. 2652–2663, May 2016.
- [13] M. Zribi *et al.*, "Potential applications of GNSS-R observations over agricultural areas: Results from the Glori airborne campaign," *Remote Sens.*, vol. 10, no. 8, 2018, Art. no. 1245.
- [14] Y. Jia, P. Savi, D. Canone, and R. Notarpietro, "Estimation of surface characteristics using GNSS LH-reflected signals: Land versus water," *IEEE J. Sel. Top. Appl. Earth Observ. Remote Sens.*, vol. 9, no. 10, pp. 4752–4758, Oct. 2016.
- [15] S. T. Lowe, C. Chew, J. Shah, and M. Kilzer, "An aircraft wetland inundation experiment using GNSS reflectometry," *Remote Sens.*, vol. 12, no. 3, 2020, Art. no. 512.
- [16] R. Imam, M. Pini, G. Marucco, F. Dominici, and F. Dovis, "UAV-based GNSS-R for water detection as a support to flood monitoring operations: A feasibility study," *Appl. Sci.*, vol. 10, no. 1, 2020, Art. no. 210.
- [17] M. Unwin, P. Jales, J. Tye, C. Gommenginger, G. Foti, and J. Rosello, "Spaceborne GNSS-reflectometry on Techdemosat-1: Early mission operations and exploitation," *IEEE J. Sel. Top. Appl. Earth Observ. Remote Sens.*, vol. 9, no. 10, pp. 4525–4539, Oct. 2016.
- [18] C. S. Ruf *et al.*, "A new paradigm in earth environmental monitoring with the CYGNSS small satellite constellation," *Sci. Rep.*, vol. 8, no. 1, pp. 1–13, 2018.
- [19] C. Chew, R. Shah, C. Zuffada, G. Hajj, D. Masters, and A. J. Mannucci, "Demonstrating soil moisture remote sensing with observations from the UK techdemosat-1 satellite mission," *Geophys. Res. Lett.*, vol. 43, no. 7, pp. 3317–3324, 2016.
- [20] P. Ferrazzoli, L. Guerriero, N. Pierdicca, and R. Rahmoune, "Forest biomass monitoring with GNSS-R: Theoretical simulations," *Adv. Space Res.*, vol. 47, no. 10, pp. 1823–1832, 2011.
- [21] X. Wu and S. Jin, "GNSS-reflectometry: Forest canopies polarization scattering properties and modeling," *Adv. Space Res.*, vol. 54, no. 5, pp. 863–870, 2014.
- [22] N. Pierdicca, L. Guerriero, R. Giusto, M. Brogioni, and A. Egido, "Savers: A simulator of GNSS reflections from bare and vegetated soils," *IEEE Trans. Geosci. Remote Sens.*, vol. 52, no. 10, pp. 6542–6554, Oct. 2014.
- [23] M. Kurum, M. Deshpande, A. T. Joseph, P. E. O'Neill, R. H. Lang, and O. Eroglu, "SCoBi-Veg: A generalized bistatic scattering model of reflectometry from vegetation for signals of opportunity applications," *IEEE Trans. Geosci. Remote Sens.*, vol. 57, no. 2, pp. 1049–1068, Feb. 2019.
- [24] A. Alonso-Arroyo *et al.*, "The light airborne reflectometer for GNSS-R observations (LARGO) instrument: Initial results from airborne and rover field campaigns," in *Proc. IEEE Geosci. Remote Sens. Symp.*, 2014, pp. 4054–4057.
- [25] F. Koch, F. Schlenz, M. Prasch, F. Appel, T. Ruf, and W. Mauser, "Soil moisture retrieval based on GPS signal strength attenuation," *Water*, vol. 8, no. 7, 2016, Art. no. 276.
- [26] M. Zribi, E. Motte, P. Fanise, and W. Zouaoui, "Low-cost GPS receivers for the monitoring of sunflower cover dynamics," *J. Sensors*, vol. 2017, 2017, Art. no. 6941739.
- [27] M. Kurum, A. C. Gurbuz, C. Nelson, L. Orsini, and M. Scheider, "On the feasibility of smartphone-based interferometric GNSS reflectometry," in *Proc. Pac. PNT Meeting*, 2019, pp. 635–640.
- [28] S. Malkos, "User location takes center stage in new android OS: Google to provide raw GNSS measurements," *GPS World*, vol. 27, no. 7, 2016, Art. no. 36.
- [29] M. Kurum, A. C. Gurbuz, and M. M. Farhad, "GNSS reflectometry from smartphones: Testing performance of in-built antennas and GNSS chips," in *Proc. IEEE Geosci. Remote Sens. Symp.*, to be published.
- [30] A. A. Serra, P. Nepa, G. Manara, and R. Massini, "A low-profile linearly polarized 3d PIFA for handheld GPS terminals," *IEEE Trans. Antennas Propag.*, vol. 58, no. 4, pp. 1060–1066, Apr. 2010.
- [31] U. Robustelli, V. Baiocchi, and G. Pugliano, "Assessment of dual frequency GNSS observations from a Xiaomi Mi 8 android smartphone and positioning performance analysis," *Electronics*, vol. 8, no. 1, 2019, Art. no. 91.



Mehmet Kurum (Senior Member, IEEE) received the B.S. degree in electrical and electronics engineering from Bogazici University, Istanbul, Turkey, in 2003, and the M.S. and Ph.D. degrees in electrical engineering from George Washington University, Washington, DC, USA, in 2005 and 2009, respectively.

He held a Postdoctoral position with the Hydrological Sciences Laboratory, NASA Goddard Space Flight Center, Greenbelt, MD, USA. In 2016, he was an Assistant Professor with the Department of Electrical and Computer Engineering, Mississippi State University, Mississippi State, MS, USA. His research interests include microwave and millimeter-wave remote sensing, RF sensors and systems, radiation and scattering theory, and signals of opportunity.

Dr. Kurum was a recipient of the Leopold B. Felsen Award for excellence in electromagnetic, in 2013 and the International Union of Radio Science (URSI) Young Scientist Award, in 2014. He is an Early Career Representative for the International URSI Commission F (Wave Propagation and Remote Sens.).



Md. Mehedi Farhad is currently working toward the Ph.D. degree in electrical and computer engineering from Mississippi State University, Mississippi State, MS, USA.

His research encompasses investigating GNSS-R techniques using low-cost and smart devices.



Ali Cafer Gurbuz (Senior Member, IEEE) received the B.S. degree in electrical and electronics engineering from Bilkent University, Ankara, Turkey, in 2003, and the M.S. and Ph.D. degrees in electrical and computer engineering from Georgia Institute of Technology, Atlanta, GA, USA, in 2005 and 2008, respectively.

From 2003 to 2008, he researched multimodal landmine detection systems as a Graduate Research Assistant and, from 2008 to 2009, as Postdoctoral Fellow, all with Georgia Institute of Technology, Atlanta, GA, USA. As an Assistant Professor (2009–2013) and an Associate Professor (2013–2016) of Electrical and Electronics Engineering with the TOBB University of Economics and Technology, Ankara, Turkey, he pursued an active research program on the development of sparse signal representations, compressive sensing theory and applications, radar and sensor array signal processing, and machine learning. He is currently an Assistant Professor with the Department of Electrical and Computer Engineering, Mississippi State University, Mississippi State, MS, USA.

Dr. Gurbuz is the author of more than 20 journals and 40 conference publications. He is the recipient of The Best Paper Award for Signal Processing Journal, in 2013 and Turkish Academy of Sciences Best Young Scholar Award in Electrical Engineering, in 2014. He was an Associate Editor for *Digital Signal Processing* and the *EURASIP Journal on Advances in Signal Processing*.